Interpreting hemoglobin and water concentration, oxygen saturation, and scattering measured *in vivo* by near-infrared breast tomography

Subhadra Srinivasan*, Brian W. Pogue*†, Shudong Jiang*, Hamid Dehghani*, Christine Kogel‡, Sandra Soho‡, Jennifer J. Gibson§, Tor D. Tosteson§, Steven P. Poplack‡, and Keith D. Paulsen*

*Thayer School of Engineering, Dartmouth College, Hanover, NH 03755; and Departments of ‡Diagnostic Radiology and §Community and Family Medicine, Dartmouth–Hitchcock Medical Center, Lebanon, NH 03756

Edited by Britton Chance, University of Pennsylvania School of Medicine, Philadelphia, PA, and approved July 29, 2003 (received for review May 11, 2003)

Near-infrared spectroscopic tomography was used to measure the properties of 24 mammographically normal breasts to quantify whole-breast absorption and scattering spectra and to evaluate which tissue composition characteristics can be determined from these spectra. The absorption spectrum of breast tissue allows quantification of (*i*) total hemoglobin concentration, (*ii*) hemoglobin oxygen saturation, and (*iii*) water concentration, whereas the scattering spectrum provides information about the size and number density of cellular components and structural matrix elements. These property data were tested for correlation to demographic information, including subject age, body mass index, breast size, and radiographic density. Total hemoglobin concentration correlated inversely to body mass index, likely because lower body mass indicates proportionately less fat and more glandular tissue, and glandular tissue contains greater vascularity, hence, more total hemoglobin. Optical scattering was correlated to breast diameter, subject age, and radiographic density. In the radiographic density, fatty breasts had low scattering power and extremely dense breasts had higher values. This observation is consistent with low attenuation of conventional x-rays with fat and higher attenuation in glandular tissues. Optically, fatty tissues have large scatterers leading to a low scattering power, whereas glandular or fibrous tissues have more cellular and collagen-based structures that lead to high scattering power. The study presents correlative data supporting the hypothesis that optical measurements of absorption and scattering can provide physiologically relevant information about breast tissue composition. These breast constituents vary significantly between individuals and can be altered because of changes in breast physiology or pathological state.

The breast is a highly heterogeneous and dynamically complex organ whose characteristics depend on factors such as age, hormonal status, habitus, family and medical history, and genetics (1–3). Normal breast tissue changes considerably during development, pregnancy, and menopause, and throughout the menstrual cycle. It has been documented that blood flow can increase up to 50% at the time of ovulation; and by the end of the monthly cycle, some women may undergo breast enlargement of up to 20% because of increased vascularity and water content (1). Total blood content can vary up to a factor of 5 or more between women based on their body-fat content, making the breast one of the most physiologically variable tissues in the human body. With near-infrared (NIR) spectral imaging, hemoglobin concentration, oxygen saturation, and water content can yield information about the current physiological state of the normal breast.

The relatively good transparency of tissue in the red and NIR spectrum (i.e., 600–1,000 nm) permits sufficient light penetration to detect signals through as much as a dozen centimeters of the breast. In the NIR spectrum, the primary absorbers of light are hemoglobin, oxyhemoglobin, water, and lipids. With knowledge of accurate spectra of these chromophores over the desired wavelengths, it becomes possible to noninvasively assess their concentration (4, 5) and, hence, total hemoglobin (Hb_T) and tissue oxygen saturation (S_tO_2).

The range of NIR technologies that have been used to measure breast tissue varies significantly, yet the findings for breast composition with NIR are fairly consistent, as summarized here. Suzuki *et al.* (6) studied the spectral transmission of normal breast in a Japanese population with a time-resolved optical system by using a single wavelength and showed variations in absorption and scattering properties with age and body mass index (BMI). Quaresima *et al.* (7) investigated spectral fitting of chromophores in the breasts of five subjects and reported variations in Hb_T, S_tO_2, water, and lipids in the following ranges: Hb_T, 2.9–20.4 μM; S_tO_2, 0–90%; water fraction, 11–74%; and lipid fraction, 26–90%. Cerussi *et al.* (8) acquired measurements from 28 subjects at seven wavelengths by using a frequency-domain, photon migration system to sample a depth of a few centimeters in normal breast tissue. They found differences in composition between premenopausal and postmenopausal superficial breast tissue and correlations in water and lipid content with age. Pogue *et al.* (9) presented results, again by using spectra from the literature, to evaluate measurements at four or five wavelengths from a frequency-domain system that imaged the whole breast. They reported typical quantitative values for hemoglobin concentration ranging from 10 to 60 μM. Shah *et al.* (10) described spectroscopy studies of superficial breast tissue in 14 subjects by using measurements at four wavelengths and showed differences in the physiological properties between premenopausal women, postmenopausal women, and women using hormone replacement therapy, where the hemoglobin content of premenopausal breast tissue was found to be highest relative to subjects with hormone replacement therapy and postmenopausal tissue, which were intermediate and lowest of the three groups, respectively. Durduran *et al.* (11) in a recent study of the healthy breast evaluated 52 volunteers in a parallel-plate transmission geometry by using three wavelengths. Their results showed correlation of BMI to blood volume and μ_s' under the assumption that the breast water fraction was fixed at 31%.

All these results have been based on either constraining the chromophores being considered in the analysis (e.g., fixed water fraction) or using complete spectral estimation but with data from only the superficial portion of the breast (e.g., NIR spectroscopy). In the study reported here, measurements of the whole breast have been achieved with spectral decomposition requiring no assumptions about chromophore concentrations. Molar absorption spectra were also determined with the imaging system used for clinical data collection. Specifically, a frequency-domain diffuse tomography system recorded intensity and phase shift of light signals through the breast in three contiguous 1-cm sections, where a diffusion model of light transport underpins the estimation of the absorption

This paper was submitted directly (Track II) to the PNAS office.

Abbreviations: NIR, near-infrared; Hb_T, total hemoglobin; S_tO_2, tissue oxygen saturation; BMI, body mass index; pO_2, partial pressure of oxygen.

†To whom correspondence should be addressed. E-mail: pogue@dartmouth.edu.

(μ_a) and transport scattering (μ_s') coefficients. The absorption coefficient spectra, $\mu_a(\lambda)$, are used to infer the concentrations of hemoglobin, oxyhemoglobin, and water by using the extinction spectra of these constituents, whereas the scattering coefficient spectra, $\mu_s'(\lambda)$, are fit with a simplified Mie theory to derive scattering power and amplitude estimates that are related to structural particle size and density in the breast (9, 12).

In this study, a cohort of 24 healthy subjects with different radiographic densities were imaged with the goal of achieving accurate spectral analysis of the whole breast. The molar absorption spectra specific to hemoglobin, oxyhemoglobin, and water were measured directly in the tomographic system to compensate for systemic errors or offsets related to diffusion-based imaging. The system sensitivity to low partial pressure of oxygen (pO_2) and low Hb_T values has been systematically tested, and a spectral fitting procedure was adopted that provided the best quantitative estimate of the optically derived physiological parameters in the normal breast. In particular, the spectrally decomposed concentrations were tested for correlation to each subject's BMI and radiographic density. These measurements mark the *in vivo* quantitative interpretation of the whole-breast concentrations of Hb_T, S_tO_2, water, and optical scattering. The long-term goal of this investigation of NIR in the breast is to explore the typical composition of and variability in the normal tissues that can be measured with NIR tomography and to determine which of the imaged quantities may be used as markers of disease (i.e., breast carcinoma), risk of disease, or response to therapeutic intervention.

Materials and Methods

Tomography System. Complete details of the imaging system design can be found in refs. 13 and 14; briefly, the automated NIR spectroscopy device was constructed to perform cross-sectional imaging of the breast by means of fiber optic bundles. The fibers arranged in a circular array (with both radial and vertical degrees of freedom) have the capability to collect data in three slices of tissue from sets of 16 source and 15 detector locations. Intensity-modulated light at six discrete wavelengths between 660 and 850 nm is used to allow multispectral interrogation of the breast. Detection is accomplished by high-gain, high-bandwidth photomultiplier tubes, and the detected light is electrically mixed with a reference signal to yield a low-frequency (500 Hz) signal that is recorded by the computer.

The measured data are calibrated to account for small offsets due to source–detector fiber transmission, alignment characteristics, and errors in discretization or model–data mismatch. By fitting the measurements to a homogenous calculation of the diffusion equation on a circular geometry (of relevant size), an initial estimate of the optical properties can be obtained. This initial estimate is used in the reconstruction on which the calibrated data are processed by a finite-element model of the optical diffusion equation in the frequency domain. The absorption and reduced scattering coefficients at each point in the breast are obtained by minimization (χ^2) of the difference between the measured and calculated fluence rate intensity and phase. An in-depth description of the reconstruction can be found in refs. 15 and 16.

Spectral Estimation of Physiologic Parameters. After reconstruction of absorption and scattering coefficient images at all six wavelengths, the absorption coefficient spectra at each location are converted to hemoglobin concentration, oxygen saturation, and water maps by using the molar absorption spectra (ε) of the chromophores assumed to be present. A linear least-squares constrained fit to the relationship $[\mu_a] = [\varepsilon][c]$ is used to obtain the average breast oxyhemoglobin, deoxyhemoglobin, and water content. Here, c refers to the concentration of the three chromophores; $[\varepsilon]$ is a 6×3 matrix of molar absorption values for six wavelengths and three chromophores, and μ_a is the vector of reconstructed (total) absorption coefficients at each wavelength. Some uncertainty exists regarding the absorption from lipids in this spectral region. Recent studies have suggested that the effect, if present, is minimal (20); hence, the absorption due to lipids is not included in our analysis.

The scattering coefficient also provides physiological information (8, 21). From an approximation to Mie scattering theory, it is possible to derive a relation between reduced scattering coefficient and wavelength λ (22, 23), given by $\mu_s'(\lambda) = A\lambda^{-SP}$, where SP is the scattering power (related to the scattering center size and number density) and A is an amplitude factor (which also depends on scatterer size and number density). The scattering power may reflect variations in breast physiologic composition associated with age and radiographic density due to variations in scattering center sizes. Typically, large scatterers have lower SP and A values, whereas small scatterers have higher SP and A coefficients (23, 24).

Phantom Experiments. For accurate chromophore concentrations, it is preferable to measure the molar absorption spectra specifically within the system being used clinically to compensate for systematic errors in the model-based estimation of concentrations. Intralipid (KabiVitrum, Stockholm) solutions were prepared with 1% lipid fraction, by volume, in sterile saline with whole blood added in varying concentrations. This solution was held in a plastic cup and positioned in the imaging array to mimic the scattering and absorption properties of breast tissue. Measurements were carried out at specific blood concentrations increased successively between 0% and 1%, in steps of 0.2%. The same type of solution was prepared a second time and deoxygenated (by addition of yeast), and the experiment was repeated. The slopes of the graphs of μ_a versus blood concentration for the two solutions yield the molar absorption coefficients for oxygenated and deoxygenated blood at each wavelength, which were converted to the corresponding values for oxyhemoglobin and deoxyhemoglobin by dividing by the hemoglobin concentration within the blood sample as measured in a clinical co-oximeter (25). The molar absorption due to pure water was determined by extra polation of the data to zero blood concentration at each wavelength. The experiments were carried out four times for oxygenated and deoxygenated solutions to obtain repeatable data sets, and the mean has been used as the molar absorption spectrum in this study.

To test the sensitivity of the system to low pO_2 values, which are typically found in tumors, the oxygen dissociation curve (i.e., Hill curve) was estimated. This involved obtaining oxygen saturation values for a complete range of pO_2 values from 150 to 0 mmHg (1 mmHg = 133 Pa) for a liquid phantom solution of 1% Intralipid and

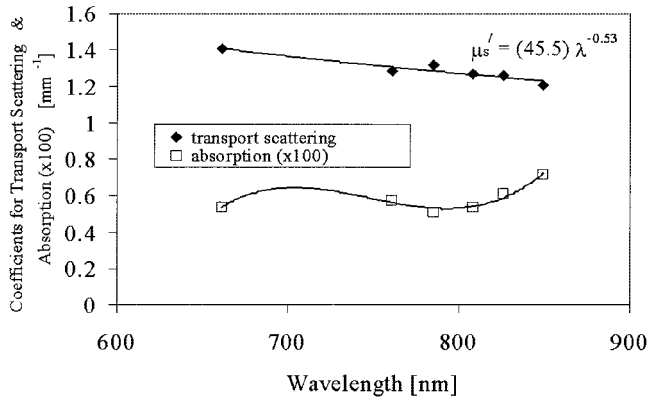

Fig. 1. Measured absorption and transport (or reduced) scattering coefficient spectrum of a single subject's breast tissue. The data points represent the average value throughout the breast, and the lines are the best-model fits to the data. The equation for scattering shows the parameters for the optimal fit to the scattering power equation.

Table 1. Mean, standard deviation, and total range of the subject clinical and NIR parameters

Property	Mean ± SD	Total range
Age, yr	53.5 ± 10	41–74
Breast diameter, mm	80 ± 13	49–102
BMI, kg/m^2	25 ± 4	19–34
Hb_T, μM	22 ± 8	9–41
S_tO_2, %	58 ± 9	32–75
Water, %	48 ± 12	21–82

1% whole blood in saline. The pO_2 was measured by using a chemical microelectrode after calibration (overnight in saline solution). By varying the pO_2 gradually by using a small amount of yeast and making measurements continually until the pO_2 reduced to zero, we obtained a complete set of data over the required range, which was compared with the theoretical Hill curve for hemoglobin.

Human Subjects. In this study, the spectral analysis of breast composition was carried out on data measured from the breasts of 24 healthy female subjects. The clinical examinations were approved by the institutional committee for the protection of human subjects, and written consent was obtained from all participating women. The age range was 41–75 years. Nine of the women were premenopausal, and 15 were postmenopausal. Nine of the postmenopausal women were taking some form of hormone replacement therapy. The participants had differing radiographic densities, and none of the subjects were known to have any form of breast disease at the time of examination. The NIR breast examinations were carried out following procedures as described (9). Additional subject-specific information was collected including age, breast size, BMI, and radiographic density as interpreted from a recent mammography examination.

Results

System Calibration and Accuracy Testing. To validate the spectral decomposition of total absorption and scattering spectra into concentrations of hemoglobin, water, and scattering parameters, a comprehensive series of tissue-simulating phantom studies were completed. Quantitative values were derived for extinction spectra of (*i*) oxyhemoglobin, (*ii*) deoxyhemoglobin, and (*iii*) water obtained from our tomography system. The results from repeated measurements indicated a standard deviation of 6% in our ability to estimate molar absorption coefficients. These coefficients represent the most accurate estimate of the molar absorption determined from our specific imaging system.

In validation tests, tissue-simulating phantoms were deoxygenated with the addition of yeast, and measurements of absorption and scattering versus solution pO_2 were recorded at multiple times during the deoxygenation process. The oxygen saturation values obtained by using a homogeneous (single pixel) reconstruction and least-squares constrained fit are estimated to be accurate to within 7.6% with the worst accuracy occurring near zero pO_2 and highest accuracy resulting at >80% saturation. Estimates of Hb_T vary by 5% with oxygen saturation, and water concentration varies by <10% over the full range of pO_2 values.

Table 2. Pearson correlation coefficients (*r*) and *P* values for three clinical parameters

Parameters	*r*	*P*
Age and BMI	0.31	0.03
Age and diameter	0.39	0.006
BMI and diameter	0.69	<0.001

Table 3. Mean values of standardized effects for subject age, BMI, and breast diameter for each of the four radiographic density categories and a global *P* value for differences in mean effects in these variables among the density categories

	Mean effect				
Outcome	Fatty	Scattered	HD	ED	*P*
Age	0.29	1.03	−0.36	−0.05	0.009
BMI	0.82	0.12	−0.27	−0.91	0.002
Diameter	1.05	0.20	−0.50	−0.25	<0.001

HD, heterogeneous dense; ED, extremely dense.

Subject Demographic Information. The left and right breasts of 24 healthy subjects were imaged by using the NIR tomography system. A typical example of absorption and scattering coefficient data collected from the breast of one volunteer is shown in Fig. 1. From these spectral measurements, five parameters were derived from the NIR reconstruction and fitting: Hb_T, S_tO_2, water concentration, scattering power, and scattering amplitude.

Table 1 shows the mean, standard deviation, and range in the age, breast diameter, BMI, and NIR physiological parameters for all subjects. The clinical parameters turned out to have statistically significant correlations with one another, although at generally low levels, as shown in Table 2. Association between these subject characteristics and the discrete classification of radiographic density was assessed by a one-way ANOVA (Table 3), comparing the standardized means of age, BMI, and breast diameter. In each case, a strong relationship with radiographic density was demonstrated.

NIR Information Relative to Age, BMI, and Breast Diameter. To investigate how the NIR parameters relate to the clinical indicators of breast composition, they were tested for correlation with each of the subject demographic parameters. The most significant correlations are plotted for BMI, breast diameter, subject age, and radiographic density in Figs. 2–5.

Table 4 shows partial correlations between the five NIR parameters and the three clinical subject factors. These correlations were computed by using a random-effects regression model with the standardized NIR parameter as an outcome. Data from both left and right breasts were included with allowance for a possible

Table 4. Estimated partial correlations relative to demographic parameters of breast diameter, subject age, and BMI, along with confidence intervals and *P* values for testing for a nonzero partial correlation

NIR property	Subject parameter	Partial correlation (95% confidence interval)	*P*
Hb_T	Diameter	−0.08 (−0.39, 0.24)	0.64
Hb_T	Age	−0.13 (−0.48, 0.21)	0.46
Hb_T	BMI	−0.43 (−0.81, −0.04)	0.04
S_tO_2, %	Diameter	0.21 (−0.24, 0.67)	0.37
S_tO_2, %	Age	−0.46 (−0.92, −0.00)	0.06
S_tO_2, %	BMI	−0.19 (−0.71, 0.33)	0.48
Water, %	Diameter	−0.43 (−0.88, 0.02)	0.07
Water, %	Age	0.26 (−0.13, 0.65)	0.20
Water, %	BMI	−0.14 (−0.59, 0.31)	0.56
log(scatt. amp.)	Diameter	−0.40 (−0.77, −0.03)	0.04
log(scatt. amp.)	Age	−0.32 (−0.67, 0.03)	0.09
log(scatt. amp.)	BMI	0.21 (−0.19, 0.62)	0.31
Scattering power	Diameter	−0.30 (−0.60, 0.00)	0.07
Scattering power	Age	−0.36 (−0.71, −0.01)	0.05
Scattering power	BMI	0.18 (−0.20, 0.57)	0.36

scatt. amp., scattering amplitude.

*$P < 0.05$ is considered to be significantly different from a slope of zero, indicating a partial correlation between property and demographic parameter.

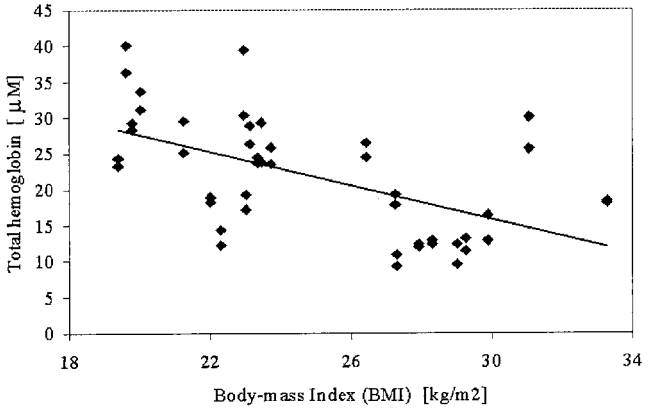

Fig. 2. Hb_T concentration (in micromolar units) is plotted against subject BMI by using data from both breasts. The solid line is a linear regression to the data showing a statistically significant correlation ($P = 0.04$ in Table 4).

correlation. The NIR parameters correlate differently to the clinical factors. Hb_T correlates significantly to BMI, whereas S_tO_2 and water correlate most significantly to age and breast diameter, respectively. The data are plotted in a representative graph in Fig. 2, which shows Hb_T as a function of BMI. The linear regression line shows the fit to the data, which is significant at the level of $P = 0.04$. Fig. 3 shows the correlations of breast diameter with water fraction plotted in Fig. 3*a* and scattering parameters plotted in Fig. 3*b*. Whereas water fraction and scattering power were close to being correlated at the level of $P = 0.05$ (actual P value was 0.07 for both),

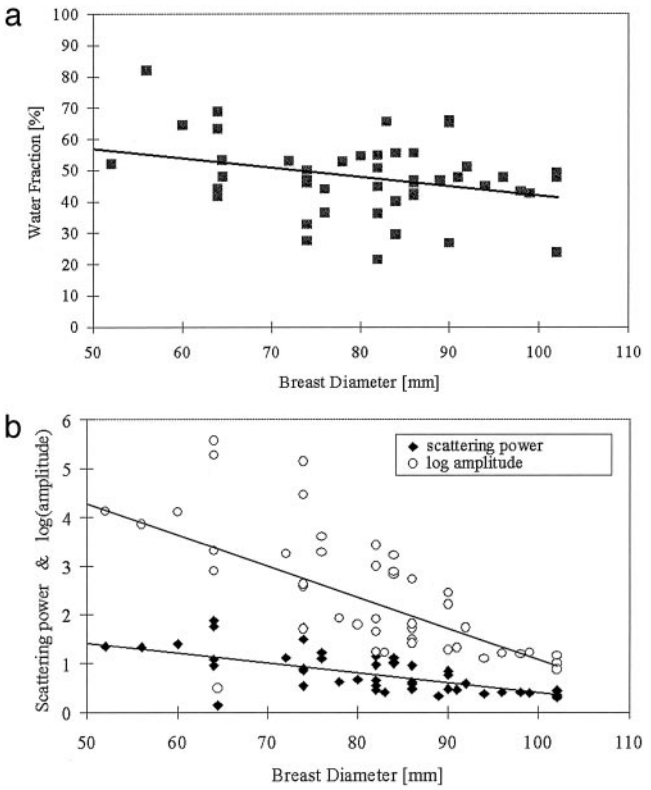

Fig. 3. (*a*) Water fraction (percentage) is plotted as a function of subject breast size, showing data points for both breasts as measured in the NIR imaging array. The solid line is a linear regression to the data. (*b*) Scattering power and amplitude are plotted against breast diameter. Amplitude has a statistically significant correlation ($P = 0.04$ in Table 4).

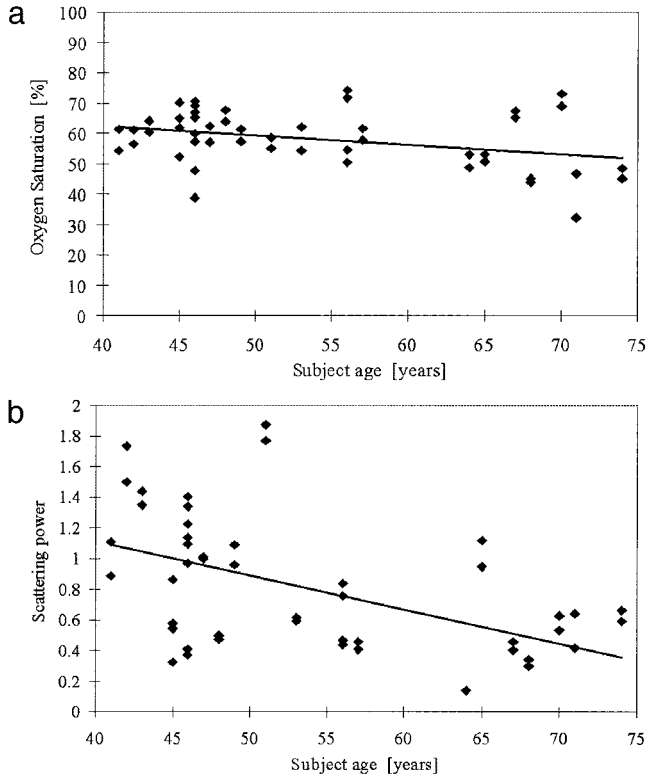

Fig. 4. (*a*) Oxygen saturation is plotted as a function of subject age, with a linear regression line shown. (*b*) Scattering power is plotted as a function of subject age, with data points for left and right breasts included. The solid line represents linear regression to the data and presents a statistically significant correlation (Table 4).

the scattering amplitude was significantly correlated at a P value of 0.04. Some indication existed that S_tO_2 may be most strongly correlated to age, as plotted in Fig. 4*a*, but the P value was 0.06. The scattering power was significantly correlated to subject age, with $P = 0.05$, as plotted in Fig. 4*b*.

NIR Information Relative to Radiographic Density. The subjects in our study were chosen with various radiographic densities. In general, it was found that the scattering amplitude appears to increase with increases in radiographic density. The statistical analysis of these data, presented in Table 5, shows that the extremely dense category was different from the fatty category for both NIR scattering parameters. It is possible that further numbers of subjects would allow a more significant discrimination among these density categories as well, based on NIR scattering. Fig. 5 shows the mean of the scattering power and amplitude for each radiographic density category. Nondense (i.e., fatty and scattered categories) breast tissue has the lowest hemoglobin and water content, whereas dense breast tissue has the highest water percentage and hemoglobin concentration. When a multivariate analysis of the data is completed, as shown in Table 5, no significant difference in Hb_T, oxygen saturation, or water content occurred among the radiographic density groups. Although hemoglobin may appear to increase with radiographic density, this increase is a result of other factors.

Trends Between NIR Parameters. It is important to assess whether duplicate or complementary information exists between the NIR parameters, themselves. A multivariate test was performed to estimate the Pearson's correlation coefficient and the P values for significance between Hb_T, S_tO_2, water, scattering power, and amplitude. The results are included in Table 6, and indicate that

Table 5. A comparison of mean standardized values for NIR properties among radiographic density groups and statistical *P* values for difference from the fatty group

NIR property	Subject radiographic density	Correlation (95% confidence interval)	Comparison with fatty group, *P*
Hb_T	Fatty	−0.22 (−0.93, 0.49)	
Hb_T	Scattered	0.45 (−0.70, 1.60)	0.42
Hb_T	Het. dense	−0.53 (−1.43, 0.37)	0.23
Hb_T	Extr. dense	0.11 (−1.27, 1.48)	0.87
S_tO_2, %	Fatty	0.40 (−0.55, 1.35)	
S_tO_2, %	Scattered	0.16 (−1.37, 1.69)	0.83
S_tO_2, %	Het. dense	0.56 (−0.65, 1.77)	0.35
S_tO_2, %	Extr. dense	0.92 (−0.90, 2.75)	0.31
Water, %	Fatty	0.09 (−0.72, 0.90)	
Water, %	Scattered	−0.02 (−1.32, 1.28)	0.98
Water, %	Het. dense	0.36 (−0.69, 1.40)	0.48
Water, %	Extr. dense	−1.20 (−2.75, 0.34)	0.12
log(scatt. amp.)	Fatty	−0.44 (−1.18, 0.29)	
log(scatt. amp.)	Scattered	−0.39 (−1.58, 0.79)	0.50
log(scatt. amp.)	Het. dense	−0.48 (−1.42, 0.46)	0.30
log(scatt. amp.)	Extr. dense	−1.60 (−3.01, −0.19)	0.03
Scattering power	Fatty	−0.57 (−1.29, 0.15)	
Scattering power	Scattered	−0.48 (−1.65, 0.69)	0.40
Scattering power	Het. dense	−0.67 (−1.58, 0.24)	0.14
Scattering power	Extr. dense	−1.76 (−3.16, −0.36)	0.02

Het., heterogeneous; Extr., extremely; scatt. amp., scattering amplitude.

Hb_T is uncorrelated to S_tO_2 and water, but statistically correlated to the two scattering parameters although with modest degrees of linearity. S_tO_2 is significantly correlated to water content with stronger linearity, but not to the scattering parameters. As expected, the scattering parameters are highly linearly correlated to each other, because they are estimated from the same model fit to the data. Fig. 6 depicts two of these trends, namely oxygen saturation versus Hb_T (i.e., uncorrelated in this data set) in *a*, and scattering power versus Hb_T in *b* (i.e., correlated in this data set with modest linearity).

Discussion

The goal of this work has been to examine the breast tissue information available from the NIR-derived measures of Hb_T, oxygen saturation, water concentration, scattering power, and scattering amplitude. These parameters are a direct consequence of tissue function and structure and should provide properties that are different from those obtained in x-ray mammography. The prelude to this study has been to ensure quantitative accuracy when imaging with our experimental system. To this end, the results have shown that the three absorption-derived measures (Hb_T, S_tO_2, and water) are separated well, without significant model-derived cross talk. The preclinical phantom measurements confirmed that we could image oxygen saturation while simultaneously imaging Hb_T and water accurately, and the data suggest that a level of less than 10% error is incurred in this situation.

An important aspect of this work is the spectral correlation with clinical characteristics such as age, breast size, and BMI based on whole-breast data. Imaging the whole breast contrasts with earlier studies that have interrogated a portion of the breast, usually the superficial regions. Results from spectroscopy studies may also misrepresent spatial changes in transmitted spectra as being related to the tissue, whereas, in some cases, they may have more to do with the exterior breast geometry. In this study, the tissue was encircled with a fiber optic array, the measurements from which were analyzed with geometry-specific numerical modeling of the light propagation, an approach thought to provide the most accurate prediction of tissue optical properties, and therefore, the most accurate prediction of whole-breast concentrations of Hb_T, HbO_2, water, and scattering.

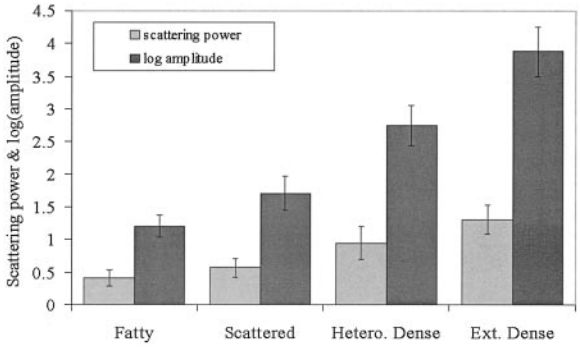

Fig. 5. NIR scattering power and amplitude are plotted as a function of the four radiographic density classifications with average values from all patients shown by the shaded bars and the standard deviation between subjects shown as the error bars. A significant difference exists between fatty and extremely dense categories for both parameters (Table 5). Hetero., heterogeneous; Ext., extremely.

The subject population studied here presented a reasonable cross-section of radiographic densities, ages, breast diameters, and BMIs. The fact that age, BMI, breast size, and radiographic density are themselves statistically correlated with modest linearity suggests that they do not yield much independent information, yet when correlating the NIR parameters to these factors we do observe significant correlations to specific clinical parameters. For example, BMI, which should provide a reasonable measure of breast fat content, is most strongly correlated to Hb_T, which would indicate a decreased amount of functional tissue involving a lower vascular density. BMI was not significantly correlated to the other NIR properties, suggesting that Hb_T provides a measurement that appears unique to the composition of the breast and one that is not possible to obtain radiographically. Further studies of Hb_T in tumors and its correlation to histologically assessed vascular density are required. Measurements in animal tissues and tumors generally confirm that Hb_T concentration as measured by NIR spectroscopy is a linear function of the total vascular density (26–28).

The scattering parameters measured from normal breast tissue also appear to yield new information. The numbers (Table 4) indicate that optical scattering (both amplitude and power) is most strongly correlated to the breast diameter, subject age, and possibly breast density. Because the structural matrix of tissue and its vascularity contribute to scattering, it would appear that age (Fig.

Table 6. Correlation coefficients among the derived NIR properties with corresponding *P* values for testing for the presence of an association between properties

	Hb_T	S_tO_2, %	Water, %	log(scatt. amp.)	Scattering power
Hb_T	1.0	0.32 ($P = 0.13$)	−0.00 ($P = 1.0$)	0.43 ($P = 0.03$)	0.45 ($P = 0.03$)
S_tO_2, %		1.0	−0.68 ($P < 0.001$)	0.05 ($P = 0.80$)	0.04 ($P = 0.87$)
Water, %			1.0	0.24 ($P = 0.03$)	0.26 ($P = 0.23$)
log(scatt. amp.)				1.0	0.99 ($P < 0.001$)

scatt. amp., scattering amplitude.

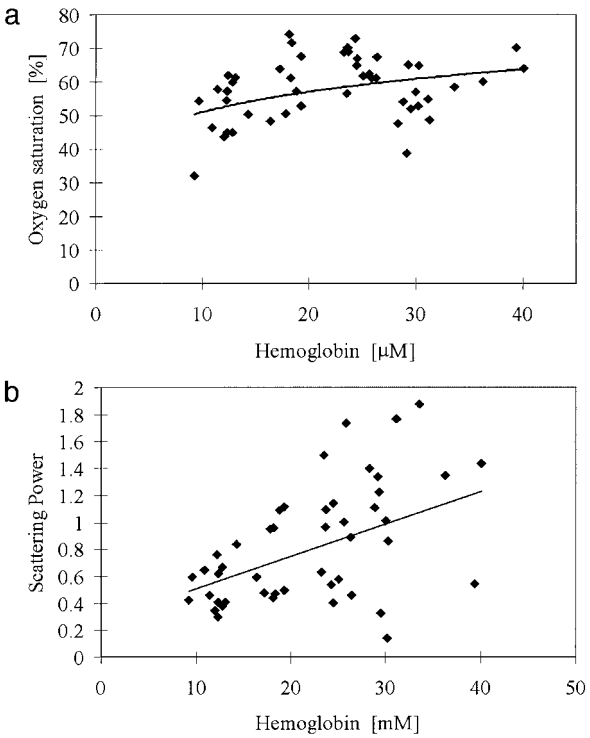

Fig. 6. Subject NIR parameters are plotted against each other. (*a*) Oxygen saturation versus Hb_T. (*b*) Scattering power versus Hb_T.

4*b*) and breast diameter (Fig. 3*a*) are major indicators of extravascular breast tissue characteristics. Further, the scattering parameters were the only ones to correlate to changes in radiographic density. This makes sense assuming that radiographic density is dominated by changes in the structural composition of the breast (i.e., fat and fibroglandular tissue components) and that these same contributions to scattering occur both in x-ray interactions (i.e., Compton scattering) and in the optical range (i.e., Mie scattering). Thus, although it could be argued that radiographic density provides a measure similar to the optical scattering coefficients, it may be that measuring the optical scattering coefficients provides a good indicator of breast density. Because breast density is strongly correlated to risk of cancer development (29), a measurement of optical scattering density may provide a nonionizing surrogate for radiodensity.

Measurement of tissue water content may be an important indicator for the breast as well. Water concentration was not correlated to any of the four clinical parameters investigated here, and was found to be uncorrelated to Hb_T (Table 6); however, indications are that it could be correlated to breast diameter ($P = 0.07$). Water content in the breast is presumably dominated by contribution from extravascular spaces, because the fraction of blood vessel volume is generally <1%; yet, the water percentages measured in these subjects were in the 40–60% range. Thus, the measurement of water is a direct indication of the water in the interstitial and cellular compartments. Studies have shown that water and fat content are inversely related, which also supports the idea that the NIR water parameter is an extravascular measurement.

The fourth NIR parameter that was recovered was oxygen saturation of the breast. This parameter did not vary much over the subject pool, which suggests that the normal breast maintains a consistent oxygen extraction fraction. The only trend that appeared to indicate possible correlation was subject age ($P = 0.06$). Further studies with more enrollments might determine whether this correlation is truly significant. In tumor tissue where metabolic imbalance is present, a reduction in oxygen saturation might be expected, and has been reported in selected cases (30). Animal studies also support the hypothesis that reduced oxygen saturation occurs in more aggressive tumors with disorganized vascular patterns (26, 31). Further study of oxygen saturation as correlated to tumor growth rate and vascular density should provide important information about the extent to which this parameter supplies unique information.

In summary, the NIR measurements indicate that the absorbing and scattering components of breast tissue all occur in different proportions within the normal subject population and that demographic trends exist that help us determine what the significance of these measurements may be. Each of the five derived parameters has a unique correlate to subject characteristics, and the trends observed can be explained by what would be expected as normal physiologic variation in the population. Further analysis of breast tissue composition and correlation to NIR spectroscopic parameters will help to firmly establish the accuracy of these measurements. Studies of how these parameters vary spatially within the breast and how they vary in pathologically altered breast tissue will also help to determine what clinical value may be present in this measurement system. Promising avenues of research may lie in the study of how Hb_T, oxygen saturation, water, and NIR scattering vary between stages or types of breast pathologies.

This work was supported by National Institutes of Health Grants PO1CA80139 and RO1CA69544.

1. Thomsen, S. & Tatman, D. (1998) *Ann. N.Y. Acad. Sci.* **838,** 171–193.
2. Stomper, P. C., Van Voorhis, B. J., Ravnikar, V. A. & Meyer, J. E. (1990) *Radiology (Easton, Pa.)* **174,** 487–490.
3. Stomper, P. C. & Gelman, R. S. (1989) *Hematol. Oncol. Clin. North Am.* **3,** 611–640.
4. Delpy, D. T. & Cope, M. (1997) *Philos. Trans. R. Soc. London B* **352,** 649–659.
5. Chance, B., Luo, Q., Nioka, S., Alsop, D. C. & Detre, J. A. (1997) *Philos. Trans. R. Soc. London B* **352,** 707–716.
6. Suzuki, K., Yamashita, Y., Ohta, K., Kaneko, M., Yoshida, M. & Chance, B. (1996) *J. Biomed. Opt.* **1,** 330–334.
7. Quaresima, V., Matcher, S. J. & Ferrari, M. (1998) *Photochem. Photobiol.* **67,** 4–14.
8. Cerussi, A. E., Berger, A. J., Bevilacqua, F., Shah, N., Jakubowski, D., Butler, J., Holcombe, R. F. & Tromberg, B. J. (2001) *Acad. Radiol.* **8,** 211–218.
9. Pogue, B. W., Poplack, S. P., McBride, T. O., Wells, W. A., Osterman, K. S., Osterberg, U. L. & Paulsen, K. D. (2001) *Radiology (Easton, Pa.)* **218,** 261–266.
10. Shah, N., Cerussi, A., Eker, C., Espinoza, J., Butler, J., Fishkin, J., Hornung, R. & Tromberg, B. (2001) *Proc. Natl. Acad. Sci. USA* **98,** 4420–4425.
11. Durduran, T., Choe, R., Culver, J. P., Zubkov, L., Holboke, M. J., Giammarco, J., Chance, B. & Yodh, A. G. (2002) *Phys. Med. Biol.* **47,** 2847–2861.
12. McBride, T. O., Pogue, B. W., Jiang, S., Osterberg, U. L., Paulsen, K. D. & Poplack, S. P. (2002) *J. Biomed. Opt.* **7,** 72–79.
13. Pogue, B. W., Testorf, M., McBride, T., Osterberg, U. & Paulsen, K. (1997) *Opt. Express* **1,** 391–403.
14. McBride, T. O., Pogue, B. W., Jiang, S., Osterberg, U. L. & Paulsen, K. D. (2001) *Rev. Sci. Instrum.* **72,** 1817–1824.
15. Jiang, H., Paulsen, K. D., Osterberg, U. L., Pogue, B. W. & Patterson, M. S. (1996) *J. Opt. Soc. Am. A* **13,** 253–266.
16. Pogue, B. W., McBride, T. O., Prewitt, J., Osterberg, U. L. & Paulsen, K. D. (1999) *Appl. Opt.* **38,** 2950–2961.
17. Pogue, B. W. & Paulsen, K. D. (1998) *Opt. Lett.* **23,** 1716–1718.
18. Schweiger, M. & Arridge, S. R. (1999) *Phys. Med. Biol.* **44,** 2703–2721.
19. Dehghani, H., Pogue, B. W., Shudong, J., Brooksby, B. & Paulsen, K. D. (2003) *Appl. Opt.* **42,** 3117–3128.
20. Cerussi, A., Jakubowski, D., Shah, N., Bevilacqua, F., Lanning, R., Berger, A. J., Hsiang, D., Butler, J., Holcombe, R. F. & Tromberg, B. J. (2002) *J. Biomed. Opt.* **7,** 60–71.
21. Cubeddu, R., D'Andrea, C., Pifferi, A., Taroni, P., Torricelli, A. & Valentini, G. (2000) *Photochem. Photobiol.* **72,** 383–391.
22. van Staveren, H. J., Moes, C. J. M., van Marle, J., Prahl, S. A. & van Gemert, M. J. C. (1991) *Appl. Opt.* **30,** 4507–4514.
23. Mourant, J. R., Fuselier, T., Boyer, J., Johnson, T. M. & Bigio, I. J. (1997) *Appl. Opt.* **36,** 949–957.
24. Bohren, C. F. & Huffman, D. R. (1983) *Absorption and Scattering of Light by Small Particles* (Wiley Interscience, New York).
25. McBride, T. O., Pogue, B. W., Gerety, E., Poplack, S., Osterberg, U. L. & Paulsen, K. D. (1999) *Appl. Opt.* **38,** 5480–5490.
26. Hull, E. L., Conover, D. L. & Foster, T. H. (1999) *Br. J. Cancer* **79,** 1709–1716.
27. Liu, H., Chance, B., Hielscher, A. H., Jacques, S. L. & Tittel, F. K. (1995) *Med. Phys.* **22,** 1209–1217.
28. Firbank, M., Okada, E. & Delpy, D. T. (1997) *Phys. Med. Biol.* **42,** 465–477.
29. Mandelson, M. T., Oestreicher, N., Porter, P. L., White, D., Finder, C. A., Taplin, S. H. & White, E. (2000) *J. Natl. Cancer Inst.* **92,** 1081–1087.
30. Tromberg, B. J., Coquoz, O., Fishkin, J. B., Pham, T., Anderson, E. R., Butler, J., Cahn, M., Gross, J. D., Venugopalan, V. & Pham, D. (1997) *Philos. Trans. R. Soc. London B* **352,** 661–668.
31. Liu, H. L., Song, Y. L., Worden, K. L., Jiang, X., Constantinescu, A. & Mason, R. P. (2000) *Appl. Opt.* **39,** 5231–5243.